



Universiteit
Leiden
The Netherlands

Ruthenium-based PACT agents based on bisquinoline chelates: synthesis, photochemistry, and cytotoxicity

Busemann, A.; Flaspohler, I.; Zhou, X.Q.; Schmidt, C.; Götzfried, S.K.; Rixel, V.H.S. van; ... ; Bonnet, S.A.

Citation

Busemann, A., Flaspohler, I., Zhou, X. Q., Schmidt, C., Götzfried, S. K., Rixel, V. H. S. van, ... Bonnet, S. A. (2021). Ruthenium-based PACT agents based on bisquinoline chelates: synthesis, photochemistry, and cytotoxicity. *Journal Of Biological Inorganic Chemistry*, 26(6), 667-674. doi:10.1007/s00775-021-01882-8

Version: Publisher's Version
License: [Creative Commons CC BY 4.0 license](#)
Downloaded from: <https://hdl.handle.net/1887/3264179>

Note: To cite this publication please use the final published version (if applicable).



Ruthenium-based PACT agents based on bisquinoline chelates: synthesis, photochemistry, and cytotoxicity

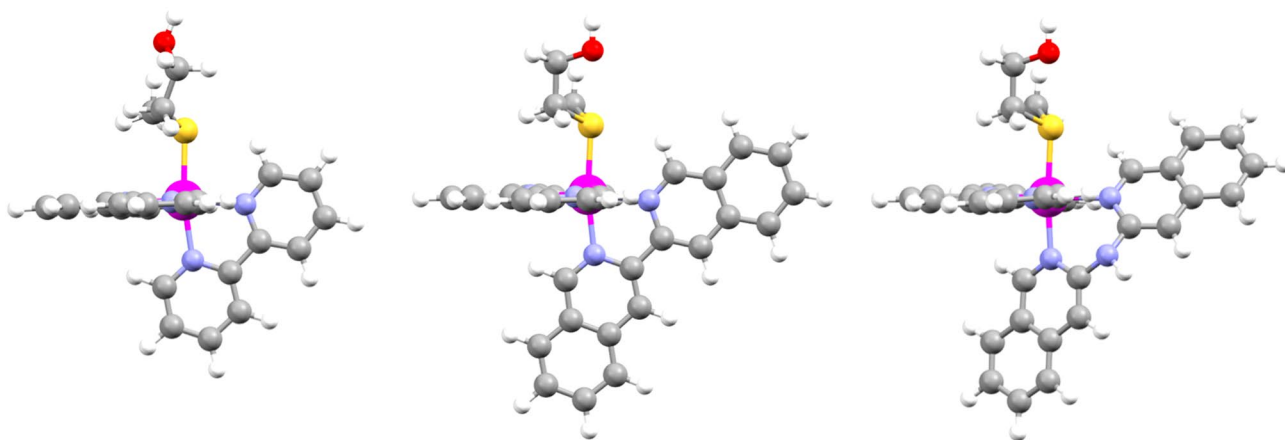
Anja Busemann¹ · Ingrid Flaspohler¹ · Xue-Quan Zhou¹ · Claudia Schmidt² · Sina K. Goetzfried¹ · Vincent H. S. van Rixel¹ · Ingo Ott² · Maxime A. Siegler³ · Sylvestre Bonnet¹

Received: 22 April 2021 / Accepted: 12 July 2021 / Published online: 10 August 2021
© The Author(s) 2021

Abstract

The known ruthenium complex $[\text{Ru}(\text{tpy})(\text{bpy})(\text{Hmte})](\text{PF}_6)_2$ (**1**)(PF_6)₂, where tpy = 2,2':6',2''-terpyridine, bpy = 2,2'-bipyridine, Hmte = 2-(methylthio)ethanol) is photosubstitutionally active but non-toxic to cancer cells even upon light irradiation. In this work, the two analogs complexes $[\text{Ru}(\text{tpy})(\text{NN})(\text{Hmte})](\text{PF}_6)_2$, where NN = 3,3'-biisoquinoline (i-biq, **2**)(PF_6)₂) and di(isoquinolin-3-yl)amine (i-Hdiqa, **3**)(PF_6)₂), were synthesized and their photochemistry and phototoxicity evaluated to assess their suitability as photoactivated chemotherapy (PACT) agents. The increase of the aromatic surface of **2**(PF_6)₂ and **3**(PF_6)₂, compared to **1**(PF_6)₂, leads to higher lipophilicity and higher cellular uptake for the former complexes. Such improved uptake is directly correlated to the cytotoxicity of these compounds in the dark: while **2**(PF_6)₂ and **3**(PF_6)₂ showed low EC₅₀ values in human cancer cells, **1**(PF_6)₂ is not cytotoxic due to poor cellular uptake. While stable in the dark, all complexes substituted the protecting thioether ligand upon light irradiation (520 nm), with the highest photosubstitution quantum yield found for **3**(PF_6)₂ ($\Phi_{[3]} = 0.070$). Compounds **2**(PF_6)₂ and **3**(PF_6)₂ were found both more cytotoxic after light activation than in the dark, with a photo index of 4. Considering the very low singlet oxygen quantum yields of these compounds, and the lack of cytotoxicity of the photoreleased Hmte thioether ligand, it can be concluded that the toxicity observed after light activation is due to the photoreleased aqua complexes $[\text{Ru}(\text{tpy})(\text{NN})(\text{OH}_2)]^{2+}$, and thus that **2**(PF_6)₂ and **3**(PF_6)₂ are promising PACT candidates.

Graphic abstract



✉ Sylvestre Bonnet
bonnet@chem.leidenuniv.nl

Extended author information available on the last page of the article

Introduction

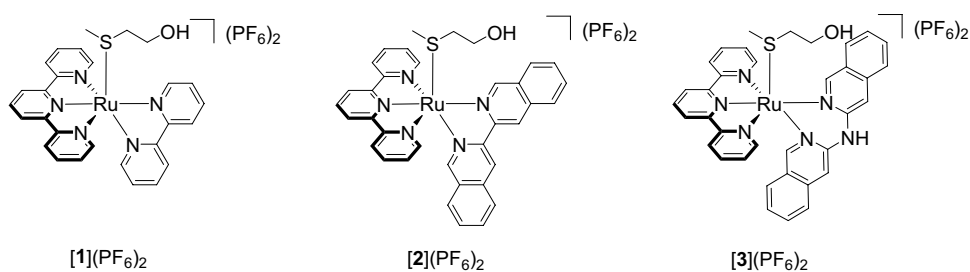
In recent years, ruthenium polypyridyl complexes gained attention in the field of phototherapy for their favorable photophysical and photochemical properties [1]. Drug activation by light irradiation at the tumor site provides physical selectivity towards cancerous tissues and minimizes the effect of the drug on the healthy, non-irradiated tissues. Therefore, undesired side effects are expected to be reduced. Two different types of phototherapy are distinguished: photodynamic therapy (PDT) and photoactivated chemotherapy (PACT). In both cases, a molecule is promoted to a singlet metal-to-ligand charge transfer excited state ($^1\text{MLCT}$) by photon absorption. From there, the molecule undergoes intersystem crossing (ISC) to a triplet metal-to-ligand charge transfer excited state ($^3\text{MLCT}$). This $^3\text{MLCT}$ state can be deactivated via four different pathways: non-radiative deactivation, emission of a photon, energy transfer to molecular oxygen to generate singlet oxygen ($^1\text{O}_2$), or thermal population of a low-lying triplet metal-centered excited state (^3MC), which leads to ligand photosubstitution [1–7]. In PDT, the production of $^1\text{O}_2$ leads to serious oxidative damage of the cells, culminating in cell death. In PACT, on the other hand, the pro-drug, which is usually poorly toxic in the dark, is activated by ligand photosubstitution [6, 8–12]. The activated drug becomes capable of interacting with biomolecules, causing cell death in an oxygen-independent way [7, 10, 13–16]. Since thermal promotion from the photochemically generated $^3\text{MLCT}$ state into the photosubstitutionally active ^3MC state is a competitive pathway for the quenching of the $^3\text{MLCT}$ state, good PACT agents are usually not emissive and produce only small amounts of $^1\text{O}_2$ [17].

To be a promising PACT agent, a metal complex has to fulfill three criteria: (1) it should be thermally stable in solution in the dark, (2) it should be photoactivatable with acceptable photosubstitution quantum yields, typically in the order of $\Phi \sim 0.01$ – 0.05 , and (3) it should show an increased cytotoxicity after light activation, compared to the dark. For example, $[\text{Ru}(\text{tpy})(\text{bpy})(\text{Hmte})](\text{PF}_6)_2$ (**1**) (PF_6)₂, where tpy = 2,2':6',2''-terpyridine, bpy = 2,2'-bipyridine, and Hmte = 2-(methylthio)ethanol, is known to

undergo photosubstitution of the thioether Hmte ligand under blue light irradiation, to generate an aqua ruthenium-based photoproduct $[\text{Ru}(\text{tpy})(\text{bpy})(\text{OH}_2)]^{2+}$ [18] that is known to be non-cytotoxic [19]. It is hence a good example for a *chemically* activated compound, i.e., a compound capable of photosubstitution, that is not expected to be *biologically* activated because its photoactivated product is not cytotoxic. To obtain high phototoxicity after light activation, ruthenium complexes require efficient cellular uptake, as well as some form of deleterious interaction of the activated photoproducts with biological molecules. Bi-cationic polypyridyl ruthenium complexes such as **1** (PF_6)₂ often show low cellular uptake [20], can be solved either by lowering the positive charge of the complex, e.g. via cyclometallation [21, 22], or by increasing the hydrophobicity of the ligands, e.g. by expanding the aromatic surface of its polypyridyl ligands or adding methyl groups [23, 24]. On the other hand, too lipophilic complexes may show too high dark cytotoxicity, which is a problem in phototherapy [25]. For PACT compounds, ligand expansion aimed at increasing steric hindrance and thus photosubstitution efficacy [26, 27], may also lead to distorted complex geometries, resulting in uncontrolled ligand release, thus thermal activation in the dark [18, 24, 28]. Overall, the design of a good PACT compound requires careful balancing of the lipophilicity of the complex and its photoreactivity.

In this work, two new ruthenium-based PACT compounds with the formula $[\text{Ru}(\text{tpy})(\text{NN})(\text{Hmte})](\text{PF}_6)_2$ (where NN = i-biq (3,3'-biisoquinoline), **2** (PF_6)₂; or i-Hdiqa (di(isoquinolin-3-yl)amine), **3** (PF_6)₂); Fig. 1), are reported. The increased aromatic surface of the bidentate ligands, compared to bpy, was chosen to improve cellular uptake. In addition, the dipyridylamine (Hdpa) scaffold, on which i-Hdiqa is based, has been shown to play a role in cellular uptake, compared to bpy-based systems [29]. Considering the promising results obtained with the tetrapyridyl complex $[\text{Ru}(\text{H}_2\text{biqbpy})(\text{dmsO})(\text{Cl})]^+$, where H_2biqbpy = 6,6'-bis[*N*-(isoquinolyl)-1-amino]-2,2'-bipyridine [30], an amine bridge was introduced here to the i-biq ligand resulting in the i-Hdiqa analog, thereby extending the family of $[\text{Ru}(\text{tpy})(\text{NN})(\text{SRR}')]^{2+}$ complexes studied for PACT [17]. Next to cellular uptake, the enlarged aromatic rings of the ligands

Fig. 1 Chemical structures of the ruthenium-based PACT agents **1** (PF_6)₂–**3** (PF_6)₂



i-biq and i-Hdiqa may also enhance interaction of the complex with proteins, membranes, or DNA, which may lead to improved cytotoxicity [31]. The monodentate thioether ligand Hmte, on the other hand, provides excellent thermal stability in the dark, while offering good photochemical release [18]. The synthesis, photochemistry, cytotoxicity, and cellular uptake of these compounds are reported, and compared to that of the known complex [1](PF₆)₂.

Results and discussion

Synthesis and characterization

The bidentate ligand i-biq was obtained following a reported procedure [32]. The ligand i-Hdiqa is also known [33] and was synthesized using a Buchwald-Hartwig coupling as described for the synthesis of other dipyriddyamine derivatives in literature [34]. After purification by column chromatography, the ligand was isolated as NMR-pure solid in 48% yield. The two ruthenium-based PACT compounds [2](PF₆)₂ and [3](PF₆)₂ were synthesized following the same reaction route as for [1](PF₆)₂ (Scheme S1). In short, the bidentate ligand was first coordinated to the ruthenium precursor [Ru(tpy)(Cl)₃], before the monodentate chloride ligand was thermally substituted by the protecting thioether ligand Hmte. The desired complexes were obtained in good yield (50 and 60%, respectively), and their purity was confirmed with ¹H NMR, ¹³C NMR, and elemental analysis. [1](PF₆)₂ was found much more soluble in water (log P_{ow} = −3.28 ± 0.31), compared to [3](PF₆)₂ which had intermediate hydrophilicity (log P_{ow} = 0.45 ± 0.10), and [2](PF₆)₂ which was the most hydrophobic complex of the series (log P_{ow} = 2.10 ± 0.27, see Table S1). These values demonstrate not only the expectedly increased lipophilicity of the i-biq and i-Hdiqa ligands, compared to bpy, but also the significant polarity, compared to [2](PF₆)₂, generated in [3](PF₆)₂ by the non-coordinated amine bridge.

Single crystals suitable for X-ray structure determination of complex [2](PF₆)₂ were obtained in the dark by slow vapor diffusion of diisopropyl ether in an acetonitrile solution of the complex (Fig. 2). Selected bond lengths, angles, and torsion angles are summarized in Table 1 and are compared to those of [1](PF₆)₂ [18]. The coordination bond lengths of the i-biq complex are not significantly different from those with bpy *e.g.* Ru-N4 is 2.104(10) vs. 2.092(1) Å for [2](PF₆)₂ vs. [1](PF₆)₂. The torsion angle of the coordinated i-biq is slightly smaller than that of bpy (N4-C24-C25-N5 = 1.9(14)° vs. N4-C20-C21-N5 = 5.3(2)°, Table 1). The Hmte ligand is bound via the sulfur atom to ruthenium, with similar bond lengths for both complexes (Ru-S = 2.368(3) and 2.3690(5) for [2](PF₆)₂ and [1](PF₆)₂, respectively). As single crystals for complex [1](PF₆)₂ could not be obtained,

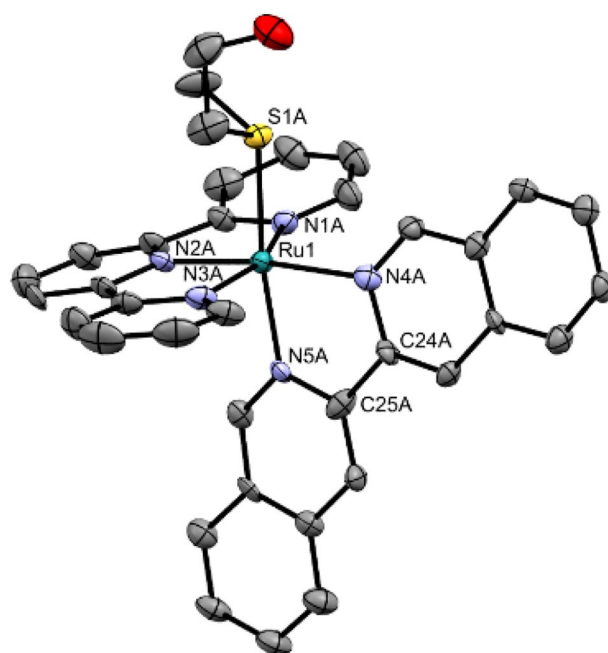


Fig. 2 Displacement ellipsoid (50% probability level) of one crystallographically independent cationic part as observed in the crystal structure of [2]²⁺. The other cation, disorder, counter ions, and H atoms have been omitted for clarity

Table 1 Selected bond lengths (Å), angles (°), and torsion angles (°) for [1](PF₆)₂–[3](PF₆)₂

	[1](PF ₆) ₂ ^a	[2](PF ₆) ₂ ^b	[1] ^{2+c}	[2] ^{2+c}	[3] ^{2+c}
Ru-S1	2.3690(5)	2.368(3)	2.394	2.396	2.396
Ru-N1	2.061(1)	2.071(9)	2.093	2.094	2.095
Ru-N2	1.961(1)	1.967(10)	1.979	1.979	1.978
Ru-N3	2.066(1)	2.073(10)	2.091	2.096	2.114
Ru-N4	2.092(1)	2.104(10)	2.116	2.117	2.138
Ru-N5	2.064(1)	2.074(9)	2.080	2.082	2.115
N1-Ru1-N2	80.08(6)	79.3(4)	79.10	79.14	79.17
N2-Ru1-N3	79.39(6)	80.1(4)	79.11	79.19	78.90
N1-Ru1-N3	159.31(6)	159.4(4)	158.06	158.17	158.01
N4-Ru1-N5	78.12(6)	79.4(4)	77.65	78.43	86.45
N4-C20-C21-N5	5.3(2)	—	—	—	—
N4-C24-C25-N5	—	1.9(14)	0.22	4.46	—
λ ^d	3.61	3.42	3.61	3.65	3.46
σ ^{2e}	57.3	58.6	62.2	60.3	46.4

^aData from Bahreman et al. [18];

^bData obtained by X-ray analysis (provided only for the crystallographically independent cation labeled A in the asymmetric unit of [2](PF₆)₂)

^cData from DFT calculations at the PBE0/TZP/COSMO level in water

^dMean quadratic elongation, where d_n is one of the six bond lengths and $\langle d \rangle$ is the mean of those bond lengths

^eBond angle variance where θ_n is one of the twelve angles

density functional theory (DFT) was used to compare the structure of $[1]^{2+}$, $[2]^{2+}$, and $[3]^{2+}$ (Fig. 2; Table S4–S6). The bond distances and angles of the DFT models of $[2]^{2+}$ and $[3]^{2+}$ are also provided in Table 1. For $[2]^{2+}$, the minimized geometry of the DFT model was very close to that of the X-ray structure. For $[3]^{2+}$, no significant differences in bond lengths or angles are found compared to $[2]^{2+}$, however, the position of the bidentate ligand towards the tpy ligand does differ. While i-biq is perpendicular to the tpy ligand, i-Hdiqa shows a characteristic bending at the amine bridge (Figure S11) [35, 36]. Calculations of the bond angle variance ($\sigma^2 = 60.3$ and 46.4 , respectively) [37], and the mean quadratic elongation ($\lambda = 3.65$ and 3.46 , respectively) [38], revealed that the octahedral geometry of both complexes is distorted, but that this distortion is mostly caused by the coordination of the tpy ligand (N1–Ru1–N3 = 158.17 and 158.01° , respectively). Overall, the extension of the bpy ligand into i-biq or i-Hdiqa does not lead to significant changes of the coordination sphere or bond lengths to the ruthenium ion.

Photochemistry

The two complexes have many overlapping $^1\text{MLCT}$ absorption bands extending between 400 and up to 600 nm, with an absorption maximum at 429 nm for $[2]^{2+}$ and a shoulder near 470 nm for $[3]^{2+}$, while for $[1](\text{PF}_6)_2$ the maximum appeared at 450 nm (Table 2; Figure S2). The low-energy transitions for $[1]^{2+}$ and $[2]^{2+}$ were very similar, confirming the electronic similarity between bpy and i-biq, while i-Hdiqa-based $[3]^{2+}$ showed overall bathochromically shifted absorption bands extending in the red region of the spectrum. The hypothesis that such a shift may be caused by the bending of the i-Hdiqa ligand, was confirmed by TDDFT calculations at the PBE0/TZP/COSMO(water) level of theory. The first significant transition ($f > 0.01$) for $[1]^{2+}$ and $[2]^{2+}$, calculated at 451 and 461 nm, respectively (Table S3), transferred an

electron from an essentially metal-centered $3d_{xz}$ to the π^* orbital centered on terpyridine (Figure S12a–b). In contrast, for $[3]^{2+}$ the metal-based 3d orbital was much more in the xy plane of the terpyridine ligand, and significantly mixed via antibonding orbital overlap with the π system of the bent quinoline moiety of the i-Hdiqa ligand (Figure S12c), thereby reducing the energy of the $^1\text{MLCT}$ transition into the terpyridine π^* -based orbital, which hence appeared at a bathochromically shifted wavelength (476 nm). Overall, in $[2]^{2+}$ the extension of the conjugation of the bpy system, compared to $[1]^{2+}$, does not significantly influence the lowest-energy $^1\text{MLCT}$ transition of the complex as this transition involves the terpyridine ligand and not the bidentate chelate, while in $[3]^{2+}$ the formation of a 6-membered metal-lacycle due to the presence of the additional NH bridge, generates a distortion of the planarity of the i-Hdiqa ligand that destabilizes the HOMO, thereby shifting the lowest-energy $^1\text{MLCT}$ transitions towards the red region of the spectrum.

Although $[2](\text{PF}_6)_2$ and $[3](\text{PF}_6)_2$ were perfectly stable in pure water in the dark at 37°C for 24 h (Figure S1a and S1b), they were clearly chemically photoactivated. Their photoreactivity was investigated upon green light irradiation (517 nm) in water at 37°C using UV–vis spectroscopy (Fig. 3). For each complex, upon irradiation a typical bathochromic shift of the absorption maximum was observed, due to the release of the thioether ligand and the formation of the corresponding aqua complex $[\text{Ru}(\text{tpy})(\text{NN})(\text{OH}_2)]^{2+}$ ($[4]^{2+}$ and $[5]^{2+}$ for NN = i-biq and i-Hdiqa, respectively, see Scheme 1) [17, 41, 42]. The formation of the aqua complexes was confirmed with mass spectrometry (Figure S4). The UV–vis spectra recorded during irradiation showed isosbestic points (at 369; 375 and 404, respectively), indicating a one-step photosubstitution reaction. The Glotaran software package was used to fit the time evolution of the UV–vis absorption spectra to a single photoreaction, and to obtain the photosubstitution quantum yields Φ_{517} (Table 2; Figure S5) [43]. The quantum yields of $[1](\text{PF}_6)_2$ and $[2](\text{PF}_6)_2$ were found similar ($\Phi_{517} = 0.022$ and 0.023 for $[1]^{2+}$ and $[2]^{2+}$, respectively). Thus, changing the bidentate ligand from bpy to i-biq did not alter the photosubstitution efficacy. However, the presence of i-Hdiqa in $[3]^{2+}$ increased the quantum yield by a 3.5-fold, to $\Phi_{517} = 0.077$, which is quite high.

The reason for the increased photosubstitution quantum yield of the Hmte ligand in $[3]^{2+}$ remains unclear. Triplet state minimization using DFT afforded, as expected, 2 different triplet states for each complex (Table S7–S12): an $^3\text{MLCT}$ state, characterized by a geometry very similar to the ground state and a highest singly occupied orbital (SOMO) located on the terpyridine ligand; and a ^3MC state, characterized by strongly elongated Ru–S and Ru–N₅^{trans} bonds (Table 3) and a highest SOMO primarily located on the metal. The difference in energy ΔE between the ^3MC

Table 2 Lowest-energy absorption maxima (λ_{max} in nm), molar absorption coefficients at λ_{max} (ϵ_{max} in $\text{M}^{-1} \cdot \text{cm}^{-1}$) in water, singlet oxygen generation quantum yields (Φ_{Δ}) in aerated methanol-*d*₄, phosphorescence quantum yields (Φ_{p}) in aerated methanol-*d*₄, and photosubstitution quantum yields upon irradiation at 517 nm (Φ_{517}) in water for complexes $[1](\text{PF}_6)_2$ – $[3](\text{PF}_6)_2$

Complex	NN	λ_{max} (ϵ_{max}) ^a	Φ_{p} ^b	Φ_{Δ} ^b	Φ_{517} ^a
$[1](\text{PF}_6)_2$	bpy	450 ($6.60 \cdot 10^3$) ^c	$< 1.0 \cdot 10^{-4\text{d}}$	$< 0.005^{\text{d}}$	0.022 ^c
$[2](\text{PF}_6)_2$	i-biq	429 ($5.76 \cdot 10^3$)	$1.5 \cdot 10^{-4}$	0.010	0.023
$[3](\text{PF}_6)_2$	i-Hdiqa	470 ($5.35 \cdot 10^3$)	$4.5 \cdot 10^{-4}$	0.042	0.077

^aIn water

^bIn methanol-*d*₄; [39]

^cData taken from Bahreman et al. [18]

^dData Busemann et al. [40]

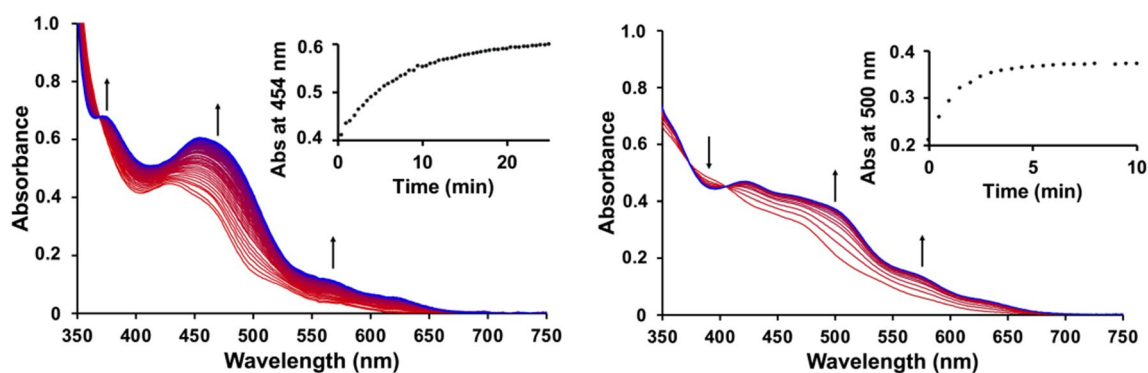
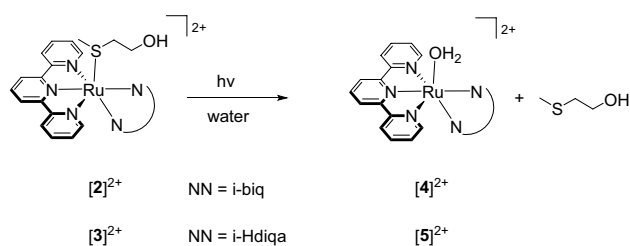


Fig. 3 Evolution of the UV–vis absorption spectra of a solution of $[2](PF_6)_2$ (left) and $[3](PF_6)_2$ (right) upon green light irradiation in water. Conditions: $[Ru]=0.074$ and 0.061 mM for $[2](PF_6)_2$ and $[3](PF_6)_2$, respectively, $T=37$ °C, light source: $\lambda=517$ nm,

$\Delta\lambda_{1/2}=23$ nm, 5.2 mW, photon flux $\Phi=5.2 \cdot 10^{-8}$ mol \cdot s $^{-1}$ for $[2](PF_6)_2$ and $[3](PF_6)_2$, $V=3$ mL, under air atmosphere. Inset: time evolution of absorbance at wavelength 454 nm for $[2](PF_6)_2$ and 500 nm for $[3](PF_6)_2$



Scheme 1 Photosubstitution of the protecting Hmte ligand in $[Ru(tpy)(NN)(Hmte)]^{2+}$ ($[2]^{2+}$ and $[3]^{2+}$) to form the corresponding aqua species $[Ru(tpy)(NN)(OH_2)]^{2+}$ ($[4]^{2+}$ and $[5]^{2+}$)

and 3MLCT states (Table 3), which is often considered as a predictive parameter for photosubstitution quantum efficiencies, did not correlate with the experimentally observed photosubstitution quantum yields. For $[2]^{2+}$ and $[3]^{2+}$ the 3MLCT state was found at a serendipitously equal energy of 190 kJ mol $^{-1}$ above their respective ground states, which corresponds to a stabilization by 31 kJ mol $^{-1}$, compared to $[1]^{2+}$ (Table 3). However, the 3MC state for $[3]^{2+}$ was found higher in energy (210 kJ mol $^{-1}$) compared to that for $[2]^{2+}$. The 3MLCT – 3MC gap energy ΔE predicted

photosubstitution quantum yields Φ_{517} to increase along the series $[3]^{2+} < [2]^{2+} < [1]^{2+}$, while the experimental trend was $[1]^{2+} \sim [2]^{2+} < [3]^{2+}$. On the one hand, this discrepancy goes in line with recent finding from the Turro group demonstrating that photosubstitution quantum yields in a series of related ruthenium complexes follow reverse energy gap law, and that population of 3MC states may not be necessary to trigger photosubstitution [44]. On the other hand, $[2]^{2+}$ and $[3]^{2+}$ have the same 3MLCT energy level, while the latter shows significantly higher photosubstitution quantum yields; other phenomena, such as interaction with the incoming solvent molecule, may also explain this discrepancy, which should be studied further. To conclude on the photochemistry, the phosphorescence of all three complexes in deuterated methanol was negligible ($\Phi_p < 5 \cdot 10^{-4}$ upon blue light irradiation), while they showed very low singlet oxygen quantum yields Φ_Δ , suggesting that their 3MLCT states might be short-lived, and that these complexes are not suitable for PDT (Table 2; Figure S3). Overall, photochemical generation of the 3MLCT state of these compounds resulted in significant ($[1]^{2+}$, $[2]^{2+}$) to high ($[3]^{2+}$) photosubstitution quantum yields, possibly *not* via thermal population of their 3MC states, while their phosphorescence and singlet

Table 3 Triplet state DFT calculations in water for complexes $[1]^{2+}$ – $[3]^{2+}$ ^a

Complex	NN	Type of triplet	Relative energy (kJ/mol)	ΔE^b (kJ mol $^{-1}$)	Ru–S (Å)	Ru–N ₅ ^{trans} (Å)	Ru–N ₄ (Å)
$[1]^{2+}$	bpy	3MLCT	221	– 25	2.401	2.077	2.102
		3MC	196				
$[2]^{2+}$	i-biq	3MLCT	190	+ 8	2.403	2.086	2.102
		3MC	198				
$[3]^{2+}$	i-Hdiqa	3MLCT	190	+ 30	2.428	2.096	2.121
		3MC	210				

^aLevel of theory: PBE0/TZP/COSMO(water)

^bDefined as $\Delta E = E(^3MC) - E(^3MLCT)$

oxygen quantum yields remained negligible. Therefore, like $[1]^{2+}$ complexes $[2]^{2+}$ and $[3]^{2+}$ fulfill the photochemical criteria of potential PACT candidates.

Cytotoxicity and cellular uptake

The thermal stability of PACT complexes is essential not only in pure water, but also in cell-growing conditions, i.e., in OptiMEM complete medium at 37 °C. All three complexes $[1](PF_6)_2$ – $[3](PF_6)_2$ were found stable for at least 24 h under such conditions (Figure S1c and S1d). In a second step, the cytotoxicity of these complexes was tested under normoxic conditions (21% O₂) in 2D monolayers of human lung carcinoma (A549) and human epidermoid carcinoma (A431) cell lines, following a protocol developed in our group [45]. In short, cancer cells were seeded at $t=0$ h, treated with six different complex concentrations at $t=24$ h, and irradiated after another 24 h with the light of a green LED for 30 min (520 nm, 38 J/cm²). The irradiation time, necessary to fully activate the complexes, was determined in a mock irradiation protocol using UV–vis spectroscopy (Figure S10). At $t=96$ h a Sulforhodamine B (SRB) assay was performed to compare the cell viability in treated vs. untreated cells (Figure S7 and S8). The effective concentrations (EC₅₀ values), i.e. the concentration at which the cell viability was reduced by 50% compared to untreated cells, are reported in Table 4. The photo index of each compound was calculated as the ratio of the EC₅₀ values obtained in the dark and upon light irradiation.

The bpy-based complex $[1](PF_6)_2$ was found as expected to be non-cytotoxic against A549 cancer cells, whether irradiated or not (EC₅₀ > 150 μM). The complexes $[2](PF_6)_2$ and $[3](PF_6)_2$ showed low cytotoxicity in the dark (80 vs. 62 μM), but revealed a significant increase in cytotoxicity

after light activation characterized by EC₅₀ values of 21 and 14 μM, respectively. These changes correspond to photo indices of ~4 for both complexes, indicating that a more cytotoxic species is released upon light activation. The released thioether ligand Hmte, tested independently, showed neither cytotoxicity in the dark nor upon light irradiation (Figure S9). In A431 cancer cells, the same trends were observed (Table 4). Therefore, the cytotoxicity observed upon light irradiation of $[2]^{2+}$ or $[3]^{2+}$ must be based on the metal-containing photoproduct, i.e. the aqua complexes $[4]^{2+}$ and $[5]^{2+}$, respectively, and not on the photoreleased Hmte ligand [46, 47].

To quantify the effect of the increased hydrophobicity of the complexes on the cellular uptake, uptake experiments were performed. A549 cells were treated with 30 μM of the complex $[1](PF_6)_2$ – $[3](PF_6)_2$, which is lower than their dark EC₅₀ values, and the ruthenium uptake was determined after 24 h incubation in the dark (Table 4). The ruthenium content in nmol Ru per mg cell protein was determined by high-resolution continuum-source atomic absorption spectrometry (HRCS AAS, further details in ESI) under normoxic (21% O₂). It should be noted here that in such an assay, we cannot distinguish aggregation of the complexes onto the cell surface, from real internalization of the complex (i.e., by passive or active crossing of the cellular membrane): the “uptake” results actually expressed the sum of both types of molecules. Complex $[1](PF_6)_2$ was less taken up (0.16 nmol per mg cell protein), compared to the other two complexes $[2](PF_6)_2$ and $[3](PF_6)_2$, for which the ruthenium uptake was 0.32 and 0.69 nmol per mg cell protein, respectively. Probably, the higher lipophilicity of $[2](PF_6)_2$ and $[3](PF_6)_2$, compared to their bpy analog, is at least partly responsible for their higher uptake. However, the more polar (log P_{ow} = 0.45) i-Hdiqa complex $[3]^{2+}$ showed enhanced

Table 4 (Photo)cytotoxicity (EC₅₀ with 95% confidence interval in μM) of $[1](PF_6)_2$, $[2](PF_6)_2$, $[3](PF_6)_2$, and Hmte in lung cancer cells (A549) and skin cancer cells (A431) under normoxic conditions (21% O₂)^a. Cellular uptake (CU in nmol Ru/mg cell protein) of $[1](PF_6)_2$ – $[3](PF_6)_2$ in lung cancer cells (A549) under normoxic conditions (21%)^b

Cell		$[1](PF_6)_2$	$[2](PF_6)_2$		$[3](PF_6)_2$		Hmte
A549	EC50,dark	> 150	79.7	+6.1 – 5.7	62.1	+16.4 – 13.8	> 150
	light	> 150	20.6	+3.0 – 2.6	13.8	+4.3 – 3.6	> 150
	PI ^c	–	3.9		4.5		–
	CU	0.16 ± 0.11	0.32 ± 0.14		0.69 ± 0.16		–
A431	Dark	> 150	55.2	+7.5 – 6.5	42.9	+9.2 – 7.5	> 150
	Light	> 150	12.2	+1.5 – 1.4	11.2	+2.7 – 2.4	> 150
	PI ^c	–	4.5		3.8		–

^aCytotoxicity experiments were performed in biological and technical triplicate; errors indicate 95% confidence intervals (in μM)

^bResults of cellular uptake (CU) experiments upon incubation for 24 h with 30 μM drug in the dark. Value is average from a biological triplicate experiment, error is the standard deviation; ^cphoto index (PI) defined as EC_{50, dark}/EC_{50, light}

accumulation, compared to its more hydrophobic *i*-biq analog $[2]^{2+}$ ($\log P_{ow} = 2.10$), so that some active transport may be involved here.

Increased uptake with polypyridyl ligands bearing a non-coordinating secondary amine group has been observed for example by Barton et al. with rhodium(III) complexes [29], or in our group by platinum(II) complexes [48]; however, the reason for such phenomenon in ruthenium(II) complexes remain unclear. Next to hypothesizing some form of active transport, we may also speculate that metal complexes bearing non-coordinated NH groups such as $[3]^{2+}$, may partly be deprotonated because of the increased acidity of the NH group upon metal coordination, which may lower the charge of the metal complex and hence improve cellular uptake by passive diffusion. For example, a concentration-dependent pKa value between 4 and 5 was reported in acetonitrile for $[Ru(\text{phen})_2(\text{HDPA})]^{2+}$ (phen = 1,10-phenanthroline, HDPA = 2,2'-dipyridylamine) [49]. We are unaware of similar pKa measurements in aqueous solution for ruthenium(II)-dipyridylamine complexes. We should also mention that for the platinum(II) complex $[Pt(\text{H}_2\text{bapbpy})]^{2+}$ (where H_2bapbpy = is N-(6-(6-(pyridin-2-ylamino)-pyridin-2-yl)pyridin-2-yl)pyridin-2-amine), a pKa of 8.3 was measured in water, which was accompanied by a massive cellular uptake in A549 lung cancer cells (1586 pmol Pt/million cells), compared to cisplatin (23 pmol Pt/million cells). However, we did not notice during our investigations on $[3]^{2+}$, any sign of deprotonation in aqueous solution near pH = 7.4, so that such arguments remain, at that moment, pure speculation. Another hypothesis is that hydrogen bonding involving the non-coordinated NH bridge and biological anions would lead to better transport of the complex through the cell membrane [50]. All in all, the difference in cellular toxicity between $[1](\text{PF}_6)_2$ on the one hand, and $[2](\text{PF}_6)_2$ and $[3](\text{PF}_6)_2$ on the other hand, probably come from other reasons than differences in cellular uptake. Clear differences of localization and/or toxicity have been observed in other published series of ruthenium polypyridyl complexes containing one or several dipyridylamine ancillary ligands [51, 52]. Probably, $[Ru(\text{tpy})(\text{bpy})(\text{OH}_2)]^{2+}$ is simply less cytotoxic than its *i*-biq and *i*-Hdiqa analogs $[4]^{2+}$ and $[5]^{2+}$, because of different cellular localization and/or interaction with biomolecules, which remains to be elucidated.

Conclusions

The chemically photoactivatable ruthenium complex $[1](\text{PF}_6)_2$ is poorly taken up by cells and showed no (photo) cytotoxicity in cancer cells. Therefore, although it is chemically activated by light it is not biologically activated by light in cells, and hence not suitable as a PACT agent. However, two analog ruthenium complexes with more hydrophobic

bidentate ligands were shown to be promising PACT compounds. $[2](\text{PF}_6)_2$ showed a photosubstitution quantum yield that was comparable with that of $[1](\text{PF}_6)_2$ and a higher cellular uptake, overall resulting in increased cytotoxicity upon green light irradiation. $[3](\text{PF}_6)_2$, which has an additional non-coordinated amine bridge, showed enhanced photosubstitution quantum yield compared to $[2]^{2+}$ and the highest cellular uptake in the series, but its photoindex was similar, in the tested conditions, to that of $[2]^{2+}$. This work demonstrates that careful considerations on ligand design are necessary to fine-tune light activation of a Ru-based PACT drug. The lipophilicity of the prodrug, which influences cellular uptake and interaction with biomolecules, must be intermediate, and its ligand exchange properties must be slow in the dark and significantly increased upon visible light irradiation.

Supplementary Information The online version contains supplementary material available at <https://doi.org/10.1007/s00775-021-01882-8>.

Acknowledgements The Netherlands Organization for Scientific Research (NWO) I kindly acknowledged for a VIDI grant to SB. The European Union is gratefully acknowledged for financial support via a Starting Grant to S. Bonnet. Prof. E. Bouwman is wholeheartedly acknowledged for support and scientific discussion.

Declarations

Conflict of interest The authors declare no conflict of interest.

Open Access This article is licensed under a Creative Commons Attribution 4.0 International License, which permits use, sharing, adaptation, distribution and reproduction in any medium or format, as long as you give appropriate credit to the original author(s) and the source, provide a link to the Creative Commons licence, and indicate if changes were made. The images or other third party material in this article are included in the article's Creative Commons licence, unless indicated otherwise in a credit line to the material. If material is not included in the article's Creative Commons licence and your intended use is not permitted by statutory regulation or exceeds the permitted use, you will need to obtain permission directly from the copyright holder. To view a copy of this licence, visit <http://creativecommons.org/licenses/by/4.0/>.

References

- Zayat L, Filevich O, Baraldo LM, Etchenique R (2013) *Philos Trans Royal Soc A Math Phys Eng Sci* 371:20120330
- Battistin F, Balducci G, Wei J, Renfrew AK, Alessio E (2018) *Eur J Inorg Chem* 2018:1469–1480
- Ragazzon G, Bratsos I, Alessio E, Salassa L, Habtemariam A, McQuitty RJ, Clarkson GJ, Sadler PJ (2012) *Inorg Chim Acta* 393:230–238
- Zayat L, Calero C, Alborés P, Baraldo L, Etchenique R (2003) *J Am Chem Soc* 125:882–883
- Sun W, Li S, Häupler B, Liu J, Jin S, Steffen W, Schubert US, Butt H-J, Liang X-J, Wu S (2017) *Adv Mater* 29:1603702
- Li A, Turro C, Kodanko JJ (2018) *Acc Chem Res* 51:1415–1421

7. Li A, Turro C, Kodanko JJ (2018) *Chem Commun* 54:1280–1290
8. Havrylyuk D, Heidary DK, Sun Y, Parkin S, Glazer EC (2020) *ACS Omega* 5:18894–18906
9. Havrylyuk D, Stevens K, Parkin S, Glazer EC (2020) *Inorg Chem* 59:1006–1013
10. Roque Iii J, Havrylyuk D, Barrett PC, Sainuddin T, McCain J, Colón K, Sparks WT, Bradner E, Monro S, Heidary D, Cameron CG, Glazer EC, McFarland SA (2020) *Photochem Photobiol* 96:327–339
11. Garner RN, Gallucci JC, Dunbar KR, Turro C (2011) *Inorg Chem* 50:9213–9215
12. Al-Afyouni MH, Rohrabough TN, Al-Afyouni KF, Turro C (2018) *Chem Sci* 9:6711–6720
13. Wei J, Renfrew AK (2018) *J Inorg Biochem* 179:146–153
14. Chan H, Ghrayche JB, Wei J, Renfrew AK (2017) *Eur J Inorg Chem* 2017:1679–1686
15. Basu U, Karges J, Chotard F, Balan C, Le Gendre P, Gasser G, Bodio E, Malacea Kabbara R (2019) *Polyhedron* 172:22–27
16. Sun W, Wen Y, Thiramanas R, Chen M, Han J, Gong N, Wagner M, Jiang S, Meijer MS, Bonnet S, Butt H-J, Mailänder V, Liang X-J, Wu S (2018) *Adv Func Mater* 28:1804227
17. Lameijer LN, Brevé TG, van Rixel VHS, Askes SHC, Siegler MA, Bonnet S (2018) *Chem A Eur J* 24:2709–2717
18. Bahreman A, Limburg B, Siegler MA, Bouwman E, Bonnet S (2013) *Inorg Chem* 52:9456–9469
19. Novakova O, Kasparkova J, Vrana O, van Vliet PM, Reedijk J, Brabec V (1995) *Biochemistry* 34:12369–12378
20. Alessio E (2017) *Eur J Inorg Chem* 2017:1549–1560
21. Lameijer LN, van de Griend C, Hopkins SL, Volbeda A-G, Askes SHC, Siegler MA, Bonnet S (2019) *J Am Chem Soc* 141:352–362
22. Huang H, Zhang P, Chen H, Ji L, Chao H (2015) *Chem A Eur J* 21:715–725
23. Schatzschneider U, Niesel J, Ott I, Gust R, Alborzinia H, Wöfl S (2008) *ChemMedChem* 3:1104–1109
24. Cuello-Garibo J-A, James CC, Siegler MA, Bonnet S (2017) *Chem Sq* 1:1–19
25. Siewert B, van Rixel VH, van Rooden EJ, Hopkins SL, Moester MJ, Ariese F, Siegler MA, Bonnet S (2016) *Chem Eur J* 22:10960–10968
26. Howerton BS, Heidary DK, Glazer EC (2012) *J Am Chem Soc* 134:8324–8327
27. Kohler L, Nease L, Vo P, Garofolo J, Heidary DK, Thummel RP, Glazer EC (2017) *Inorg Chem* 56:12214–12223
28. Lameijer LN, Ernst D, Hopkins SL, Meijer MS, Askes SH, Le Dévédec SE, Bonnet S (2017) *Angew Chem Int Ed* 56:11549–11553
29. Komor AC, Schneider CJ, Weidmann AG, Barton JK (2012) *J Am Chem Soc* 134:19223–19233
30. van Rixel VHS, Siewert B, Hopkins SL, Askes SHC, Busemann A, Siegler MA, Bonnet S (2016) *Chem Sci* 7:4922–4929
31. Han Ang W, Dyson PJ (2006) *Eur J Inorg Chem* 2006:4003–4018
32. Funayama T, Kato M, Kosugi H, Yagi M, Higuchi J, Yamauchi S (2000) *Bull Chem Soc Jpn* 73:1541–1550
33. Hou Z, Nishiura M, Rai VK (2011) Novel Complex Compound and Use Thereof. WO2012114940A1, application date 2012/08/30/, application number JP2012053392W, priority numbers JP2011038483A-2011-02-24
34. Marion R, Sguerra F, Di Meo F, Sauvageot E, Lohier J-F, Danielou R, Renaud J-L, Linares M, Hamel M, Gaillard S (2014) *Inorg Chem* 53:9181–9191
35. Toyama M, Suganoya R, Tsuduura D, Nagao N (2007) *Bull Chem Soc Jpn* 80:922–936
36. Chanda N, Mobin SM, Puranik VG, Datta A, Niemeyer M, Lahiri GK (2004) *Inorg Chem* 43:1056–1064
37. Robinson K, Gibbs GV, Ribbe PH (1971) *Science* 172:567–570
38. Fleet ME (1976) *Mineral Mag* 40:531–533
39. García-Fresnadillo D, Georgiadou Y, Orellana G, Braun AM, Oliveros E (1996) *Helv Chim Acta* 79:1222–1238
40. Busemann A, Araman C, Flaspohler I, Pratesi A, Zhou X-Q, van Rixel VHS, Siegler MA, Messori L, van Kasteren SI, Bonnet S (2020) *Inorg Chem* 59:7710–7720
41. Goldbach RE, Rodriguez-García I, van Lenthe JH, Siegler MA, Bonnet S (2011) *Chem Eur J* 17:9924–9929
42. Siewert B, Langerman M, Hontani Y, Kennis JTM, van Rixel VHS, Limburg B, Siegler MA, Talens Saez V, Kiełtyka RE, Bonnet S (2017) *Chem Commun* 53:11126–11129
43. Snellenburg JJ, Laptanok SP, Seger R, Mullen KM, Van Stokkum IH (2012) *J Stat Softw* 49:1–22
44. Loftus LM, Rack JJ, Turro C (2020) *Chem Commun* 56:4070–4073
45. Hopkins S, Siewert B, Askes S, Veldhuizen P, Zwier R, Heger M, Bonnet S (2016) *Photochem Photobiol Sci* 15:644–653
46. Cuello-Garibo J-A, Meijer MS, Bonnet S (2017) *Chem Commun* 53:6768–6771
47. Azar DF, Audi H, Farhat S, El-Sibai M, Abi-Habib RJ, Khayzer RS (2017) *Dalton Trans* 46:11529–11532
48. van Rixel VHS, Busemann A, Wissingh MF, Hopkins SL, Siewert B, van de Griend C, Siegler MA, Marzo T, Papi F, Ferraroni M, Gratterer P, Bazzicalupi C, Messori L, Bonnet S (2019) *Angew Chem Int Ed* 58:9378–9382
49. Drew MGB, Nag S, Datta D (2008) *Inorg Chim Acta* 361:417–421
50. Patil SK, Ghosh R, Kennedy P, Mobin SM, Das D (2016) *RSC Adv* 6:62310–62319
51. Putta VR, Chintakuntla N, Mallepally RR, Avudoddi S, Nancherla NKD, Surya SS, Sirasani S (2016) *J Fluoresc* 26:225–240
52. Mari C, Pierroz V, Leonidova A, Ferrari S, Gasser G (2015) *Eur J Inorg Chem* 2015:3879–3891

Publisher's Note Springer Nature remains neutral with regard to jurisdictional claims in published maps and institutional affiliations.

Authors and Affiliations

Anja Busemann¹ · Ingrid Flaspohler¹ · Xue-Quan Zhou¹ · Claudia Schmidt²  · Sina K. Goetzfried¹ · Vincent H. S. van Rixel¹ · Ingo Ott²  · Maxime A. Siegler³ · Sylvestre Bonnet¹ 

¹ Leiden Institute of Chemistry, Leiden University, Einsteinweg 55, 2333CC Leiden, The Netherlands

² Institute of Medicinal and Pharmaceutical Chemistry, Technische Universität Braunschweig, Beethovenstrasse 55, 38106 Braunschweig, Germany

³ Small Molecule X-Ray Facility, Department of Chemistry, Johns Hopkins University, Baltimore, Maryland 21218, USA